Negative ions of p-nitroaniline: Photodetachment, collisions, and ab initio calculations

Byron H. Smith, Angela Buonaugurio, Jing Chen, Evan Collins, Kit H. Bowen et al.

Citation: J. Chem. Phys. **138**, 234304 (2013); doi: 10.1063/1.4810869
View online: http://dx.doi.org/10.1063/1.4810869
View Table of Contents: http://jcp.aip.org/resource/1/JCPSA6/v138/i23
Published by the AIP Publishing LLC.

Negative ions of p-nitroaniline: Photodetachment, collisions, and *ab initio* calculations

Byron H. Smith,[1] Angela Buonaugurio,[2] Jing Chen,[2] Evan Collins,[2] Kit H. Bowen,[2] Robert N. Compton,[1,3] and Thomas Sommerfeld[4]
[1]*Department of Physics, University of Tennessee, Knoxville, Tennessee 37996, USA*
[2]*Department of Chemistry, Johns Hopkins University, Baltimore, Maryland 21218, USA*
[3]*Department of Chemistry, University of Tennessee, Knoxville, Tennessee 37996, USA*
[4]*Department of Chemistry and Physics, Southeastern Louisiana University, Hammond, Louisiana 70402, USA*

(Received 13 March 2013; accepted 28 May 2013; published online 19 June 2013)

The structures of parent anion, M^-, and deprotonated molecule, $[M-H]^-$, anions of the highly polar p-nitroaniline (*p*NA) molecule are studied experimentally and theoretically. Photoelectron spectroscopy (PES) of the parent anion is employed to estimate the adiabatic electron affinity ($EA_a = 0.75 \pm 0.1$ eV) and vertical detachment energy (VDE = 1.1 eV). These measured energies are in good agreement with computed values of 0.73 eV for the EA_a and the range of 0.85 to 1.0 eV for the VDE at the EOM-CCSD/Aug-cc-pVTZ level. Collision induced dissociation (CID) of deprotonated *p*NA, $[pNA - H]^-$, with argon yielded $[pNA - H - NO]^-$ (i.e., rearrangement to give loss of NO) with a threshold energy of 2.36 eV. Calculations of the energy difference between $[pNA - H]^-$ and $[pNA - H - NO]^-$ give 1.64 eV, allowing an estimate of a 0.72 eV activation barrier for the rearrangement reaction. Direct dissociation of $[pNA - H]^-$ yielding NO_2^- occurs at a threshold energy of 3.80 eV, in good agreement with theory (between 3.39 eV and 4.30 eV). As a result of the exceedingly large dipole moment for *p*NA (6.2 Debye measured in acetone), we predict two dipole-bound states, one at ∼110 meV and an excited state at 2 meV. No dipole-bound states are observed in the photodetachment experiments due the pronounced mixing between states with dipole-bound and valence character similar to what has been observed in other nitro systems. For the same reason, dipole-bound states are expected to provide highly efficient "doorway states" for the formation of the pNA^- valence anion, and these states should be observable as resonances in the reverse process, that is, in the photodetachment spectrum of pNA^- near the photodetachment threshold. © *2013 AIP Publishing LLC*. [http://dx.doi.org/10.1063/1.4810869]

I. INTRODUCTION

The highly polar p-nitroaniline (*p*NA) molecule captures free electrons to form the pNA^- anion while deprotonation of *p*NA occurs in solution to form the $[pNA - H]^-$ anion. This research represents a combined experimental and computational investigation of the valence (parent and deprotonated) as well as dipole-bound anions of *p*NA. p-Nitroaniline represents a classic "push-pull" aromatic molecule as a result of the electron donating NH_2 and electron accepting NO_2 moieties at the para postions on the π-conjugated benzene ring (Figure 1).[1]

Such donor-acceptor molecules show great promise as nonlinear optical crystals for a host of applications.[2] The dipole moment of p-nitroaniline has been measured in acetone to be 6.2 Debye[3] while calculations of isolated *p*NA give values between 7.0 and 8.1 Debye.[4] The dipole moment of the excited singlet state of *p*NA has been determined to be 13.35 D.[5] Such large dipole moments assure strong binding of an electron to the ground and excited states to form dipole-bound anions and electronically excited Feshbach resonances, respectively.

A number of studies have considered the negative ion properties of *p*NA. In one study, thermal electrons were found to attach to *p*NA to form a long-lived, so-called nuclear-excited or vibrationally excited Feshbach resonance with an auto-detachment lifetime of ∼15 μs.[6] Dissociative electron attachment processes at higher electron energies were not reported. Huh *et al.*[7] obtained electron affinities (EA_as) for a series of substituted benzenes by determining the electron-transfer equilibria in the gas phase using an EA_a scale established with nitrobenzene ($EA_a = 0.99$ eV)[8] to provide an absolute calibration. This method resulted in an EA_a of *p*NA to be 0.91 eV. One photoionization study of *p*NA has given an ionization potential of 8.34 ± 0.01 eV[9] while another electron impact ionization study gave an ionization potential of 8.6 eV[10] as well as reporting appearance energies for $C_6H_6N^+$ and $C_6H_6NO^+$. The former ion results from NO_2 loss and the occurrence of the latter product implies considerable rearrangement in the loss of NO. Many studies have also reported NO loss from molecules similar to *p*NA and discuss the possible rearrangement pathways.[11,12]

In this study, we present the experimental valence adiabatic electron affinity (EA_a) and vertical detachment energy (VDE) for the *p*NA parent anion by means of photoelectron spectroscopy (PES). In addition, the deprotonated *p*NA anion was produced by electrospray ionization followed by collision-induced dissociation (CID). Experimental measurements of these photodetachment and dissociation energy thresholds are compared to computed values. We also present

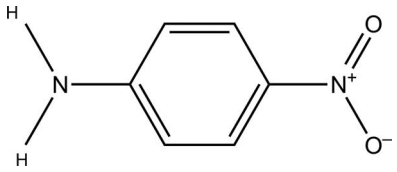

FIG. 1. Stick diagram of the p-nitroaniline molecule showing the donor (NH_2) and acceptor (NO_2) moieties responsible for the large dipole moment of this molecule.

ab initio calculations of dipole-bound vertical electron affinities for *p*NA as well as a comparison of experimental and calculated binding energies for all dipole-bound affinities reported, thus far, in the literature for polar molecules having moments from ∼2.4 to 7 Debye. The experiments to be reported in this work are not designed to detect dipole-bound anions; however, we conjecture on the possible transport of electrons through polar molecules in the gaseous and liquid state which might be facilitated by dipole-bound or quadrupole-bound anions.

II. COMPUTATIONAL AND EXPERIMENTAL METHODS

A. Photoelectron spectroscopy

PES was conducted by crossing a mass-selected negative ion beam with a fixed-frequency photon beam and energy-analyzing the resultant photodetached electrons. This technique is governed by the energy conserving relationship $h\nu = EKE + EBE$, where $h\nu$ is the photon energy, EKE is the photodetached electron kinetic energy, and EBE is the electron binding energy or the transition energy needed to take the anion to a particular vibrational state of its neutral counterpart.

Negative ions were formed by slow-electron attachment to *p*NA. The ion source was a biased (−500 V), supersonic expansion nozzle-ion source, where the *p*NA sample was placed inside its stagnation chamber and heated between 30 and 60 °C. The vapor was then co-expanded with approximately 1–2 atm of argon gas through a 25 μm nozzle into $\sim 10^{-4}$ Torr vacuum. Electron attachment occurs by injecting low energy electrons from a hot and even more negatively biased thoriated iridium filament into the expanding jet, where a weak external magnetic field helps to form a micro-plasma. The newly formed anions were then extracted, collimated, and transported via ion optics through the flight tube of a 90° magnetic sector mass spectrometer with a typical mass resolution of ∼400. The mass-selected beam of *p*NA parent anions of interest was then crossed with an intracavity operated argon ion laser beam, and the photodetached electrons were energy-analyzed by a hemispherical electron energy analyzer with a resolution of ∼30 meV. The photoelectron spectrum was recorded with 2.54 eV photons and calibrated against the well-known photoelectron spectrum of the O^- anion.[13] A detailed description of this apparatus has been described previously.[14]

B. Collision induced dissociation

All CID studies were performed with a QStar Elite triple-quadrupole mass spectrometer (ABSciex) using argon as the collision target (Figure 2). Ions were created via electrospray ionization (TurboIonSpray®) by passing a dilute solution containing the analyte through a 0.005 in. inlet syringe tip with a bias voltage of −4.2 kV and a flow rate of 20 μL/min. The resultant charged vapor was carried into the instrument by a nitrogen "curtain" gas. The ions then passed through a declustering region and focusing potential before being

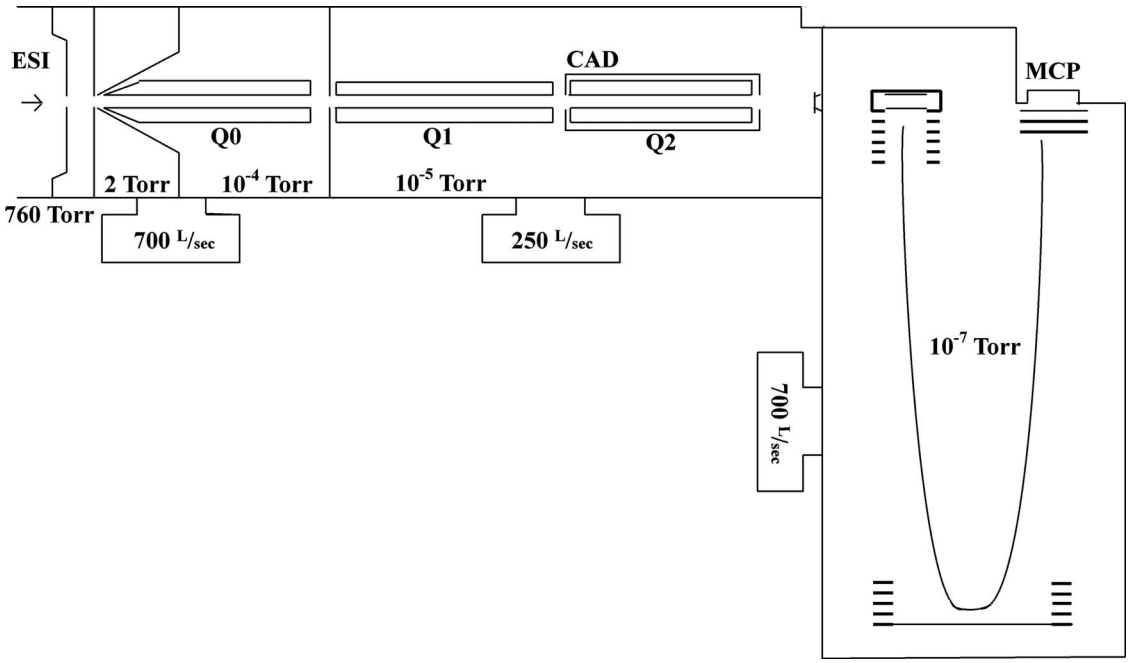

FIG. 2. Schematic of the CID apparatus (QStar Elite TOFMS) showing the quadrupole Q1 for isolation of the electrospray ions and the collision region containing argon gas (CAD) followed by product ion identification by the TOF Mass Spectrometer. Differential pumping occurs at each chamber as shown along with approximate operating pressures in each region.

spatially separated in the first of three quadrupoles (Q0), mass selected in the second quadrupole (Q1), followed by collision in the final quadrupole (Q2). The collision energy (CE) is set by the difference in potential of the first quadrupole and the offset voltage (RO2) on the sheath of the final quadrupole (CE = Q0–RO2). Final mass analysis of the collision products was performed using a reflectron time-of-flight (TOF) mass spectrometer.

The CAD pressure was held at approximately 3.5×10^{-5} Torr throughout the collision process. This is consistent with previous threshold CID experiments.[15–23] The collision cell in the QStar Elite system is 21.2 cm long which is shorter than the expected mean free path of collisions at this pressure.

Calibration of the laboratory energy for the CID studies was carried out using two procedures. First, a retardation analysis was carried out resulting in a vanishing ion signal at 0 ± 0.5 eV. In the QStar Elite system, the presence of the collision gas could not be eliminated because it is used in many of the other instrument processes such as ion cooling. In a second procedure, the energy scale was calibrated using previous studies of the tri-iodide anion, I_3^-.[15–17] Thresholds from these two methods agreed within error bars; however, the I_3^- calibration method is believed to be more precise and accurate.

Following calibration with I_3^-, a concentrated stock solution of *p*NA in methanol was prepared and further diluted ($\sim$2.5 μg/mL) for use in the electrospray ionization source. The CE was varied from 8 to 27.5 eV in steps of 0.5 eV in the lab frame.

All ion peak magnitudes were calculated by integrating the mass peak using the Analyst® software package. The cross-section was calculated as the ratio of the target's fragment peak to the sum of the parent ion's peak and the rest of the fragments' peaks. Modeling of the data was carried out using the empirical line of centers model of Armentrout *et al.*[18–23]

$$\sigma(E) = \sigma_0 \sum_i g_i \frac{(E + E_i - E_0)^n}{E}, \quad (1)$$

where E refers to the CE in the center of mass, while each E_i is an internal energy with respective Boltzmann populations, g_i. Multiplicities and corresponding Boltzmann populations were directly computed using the Beyer-Swinehart algorithm using an effective temperature of 300 K.[24] Constants σ_0, E_0, and n are fit parameters physically interpreted as a scaling factor, the threshold energy, and a factor to account for discrepancies between CID and hard-sphere collisions, respectively. To account for the thermal distribution of the collision target and the deficiency of energy transfer to the reaction coordinate from uncentered collisions, we used the method of Nalley *et al.*[25] to develop a distribution of relative velocities.

The transition state utilized in the loss of NO is characterized by the rearrangement of the nitro group to form an ONO chain prior to dissociation. After this rearrangement, the dissociation process is expected to follow a monotonically uphill fragmentation. The transition state used in the modeling of the loss of NO_2^- is a tight transition state with vibrational modes corresponding to the vibrational modes of the deprotonated molecule minus that which corresponds to the reaction coordinate. In this case, the vibrational mode corresponding to the C–N stretch of the nitro group at 1339.03 cm^{-1}. This choice was motivated by the direct cleavage process resulting in NO_2^- anions which is a purely uphill process.

Nonlinear regressions were carried out using a Bayesian Markov Chain Monte Carlo simulation with normal prior probability distributions. The mean of the priors were established by performing a coarse maximum likelihood grid search over the parameter space. In addition to parameter estimates, this fitting method allows for the calculation of model parameters without using numerical approximations to the derivatives which has been shown to be unstable in some cases of energy resolved dissociation modeling.[26] Following this procedure, the CID results in a center-of-mass threshold energy of 1.34 eV, within experimental error of the previously reported value of 1.31 ± 0.06 eV.[15–17] This means that the correction to the ion energy obtained by using the voltage difference between the ion source and target is 0.4 eV in the lab frame.

C. *Ab initio* methods

Computational investigations focused on characterizing valence and dipole-bound states of the anions of *p*NA. p-Nitroaniline is too large to use highly reliable *ab initio* methods typically required for predicting electron affinities accurately, and therefore more approximate methods must be used. An additional challenge is that self-consistent-field (SCF) calculations of the valence anion show very large spin contamination rendering second-order Møller–Plesset perturbation theory (MP2) for the valence anion calculations unreliable. Consequently, minimum energy structures and vibrational frequencies of the neutral were computed using both MP2 and the TPSS density functional,[27] while only the TPSS functional was used for the valence anion. The basis set used in these calculations is Ahlrichs's redefined triple-ζ set augmented with a minimal set of diffuse functions (ma-Def2-TZVP).[28,29]

Vertical electron affinities and vertical electron detachment energies were computed directly with the equation-of-motion coupled-cluster with single and double excitations method for electron affinities (EA-EOM-CCSD). The VDE was also computed indirectly as the difference between coupled-cluster with single, double, and perturbative triple excitations energies of the neutral and the anion (ΔCCSD(T)). Owing to the spin contamination problem in Hartree-Fock calculations for the anion, coupled-cluster calculations for the anion were performed using the orbitals of the neutral (so called QRHF coupled-cluster calculations). Two basis sets were used in the coupled-cluster calculations, Dunning's correlation consistent double-ζ (Aug-cc-pVDZ) and triple-ζ (Aug-cc-pVTZ) sets,[30,31] which were further augmented with a 6*s*6*p*6*d* set (even-tempered exponents between 0.01 and 3.16×10^{-5}) of extra diffuse functions centered at the center of mass of the molecule to characterize dipole-bound states (Aug-cc-pVDZ+ and Aug-cc-pVTZ+). In the MP2 and in all coupled-cluster calculations, the core electrons were frozen in their SCF orbitals. Three program packages were employed, GAUSSIAN09,[32] Orca,[33] and CFOUR.[34]

The adiabatic electron affinity was computed initially using the B3LYP/6-311++G* level of theory to compute both geometries and single-point energies of the neutral and the valence anion. A more robust value was obtained by combining our best estimates of the following three properties: The VDE (EOM-CCSD/Aug-cc-pVTZ), the deformation energy of the closed-shell neutral, and the zero-point correction (TPSS-DFT frequencies). GAUSSIAN03[32] was used to computationally investigate the dissociations required for the loss of NO and NO_2^-. Calculations of the dissociation energy were performed at the B3LYP/6-311++G* and MP2/Aug-cc-pVDZ levels of theory.

III. RESULTS AND DISCUSSION

A. Photoelectron spectrum

Attempts were first directed to produce the dipole-bound anion of p-nitroaniline, since its dipole moment is above both the theoretical critical value for a point dipole of 1.625 D and the empirical minimum value of 2.5 D necessary to support a stable dipole-bound state (see Ref. 35 and others cited therein). However, the dipole-bound anion of *p*NA was not evident in the photodetachment data, characterized in a photoelectron spectrum as a single, narrow peak close to zero electron binding energy (EBE) which reflects the nearly identical geometries between the anion and neutral. This dipole-bound feature was not observed due to the nozzle-ion source's tendency to produce only the most stable anionic state of a molecule, which in this case was the valence anion state of p-nitroaniline.

In our experiment, we observed the photoelectron spectrum signature of a typical valence anion and this is shown in Figure 3. This spectrum consists of a broad, unresolved band with an onset at 0.75 ± 0.10 eV and a maximum intensity at EBE 1.1 eV. The latter value corresponds to the best estimate of the VDE of the parent anion.

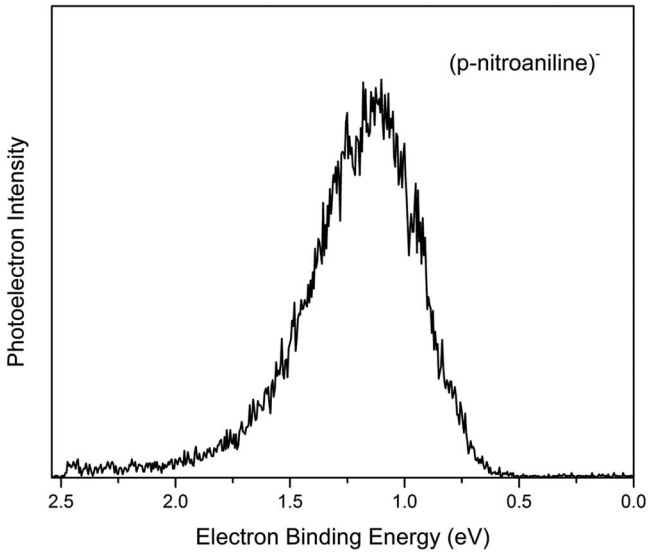

FIG. 3. The photoelectron spectrum of the valence p-nitroaniline anion recorded at 2.54 eV photons. The EA_a is estimated as the signal onset at 0.75 ± 0.1 eV and a VDE of 1.1 eV.

Photodetachment is essentially an instantaneous process; therefore the resultant photoelectron spectral profile is governed by Franck-Condon overlap between the vibrational levels of the ground electronic state of the anion (v″) and those of the ground electronic state of the neutral (v′). In the case of the *p*NA molecule, the structures of the anion and its neutral are not thought to differ greatly, suggesting that there is good overlap between the v″ = 0 and v′ = 0 levels. Nevertheless, its photoelectron spectrum exhibits little vibrational structure, making the precise assignment of the origin transition difficult. Furthermore, as evidenced by its low EBE spectral tail and the source conditions utilized, vibrational hot bands are probably present. Since vibrational hot bands often account for the first 0.1 to 0.2 eV of the low EBE tail and since there is a discernible steep rise in signal at EBE = 0.75 eV, we estimate the value of EA_a to be 0.75 ± 0.10 eV. This value is in good agreement with theoretical calculations estimate of 0.73 eV.

B. Collision induced dissociation

Figure 4 shows the deprotonated *p*NA molecule $[pNA\text{-}H]^-$, and the appearance of ions corresponding to the loss of NO and NO_2^- from $[pNA\text{-}H]^-$. The CID pathways of the $[pNA\text{-}H]^-$ anion is given below:

$$pNA\text{-}H^- \rightarrow [pNA - H - NO]^- + NO$$

and

$$pNA\text{-}H^- \rightarrow [pNA - H - NO_2] + NO_2^-$$

are listed in order of increasing energy required to induce dissociation (see Figure 5). The two fragmentation pathways observed here are commonly seen in many similar molecules.[11,12]

Calculations of the threshold for both reaction pathways were carried out with the results shown in Table I. The CRUNCH package has been used to show similar results (see the supplementary materials).[22,23,36–48] There are considerable differences in the *ab initio* thresholds depending

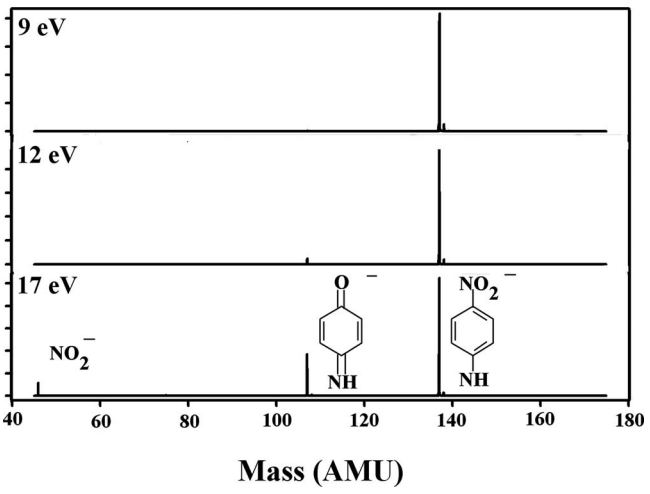

FIG. 4. Appearance of fragments caused by collision of $[pNA\text{-}H]^-$ with argon at lab frame energies of 9 eV, 12 eV, and 17 eV. Relative abundances are normalized to the parent anion peak.

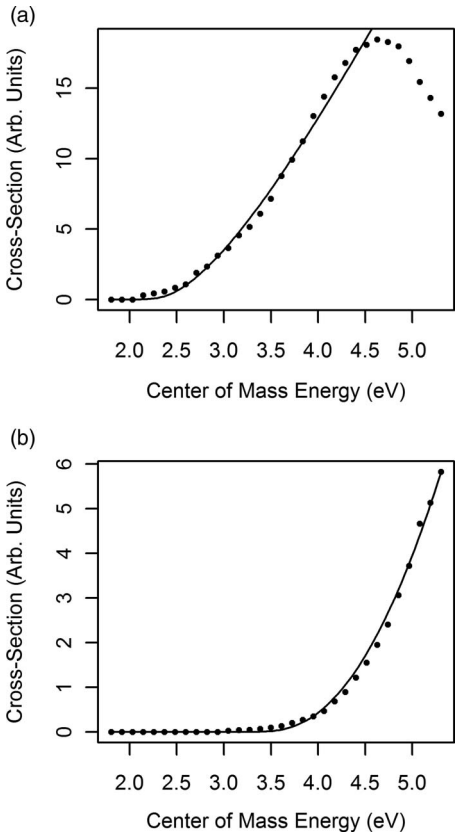

FIG. 5. Nonlinear fits of the CID cross-section of $[p\text{NA-H}]^-$ into (a) $[p\text{NA-H-NO}]^-$ and (b) NO_2^-.

upon the method employed. Despite these differences some conclusions can be drawn concerning the dissociation mechanisms.

In comparing experiment with calculations, one can see that there is good agreement between the values for the dissociation pathway leading to NO_2^- loss (pathway 2), while a significant barrier prevents the loss of NO from deprotonated *p*NA. This is attributed to the rearrangement of the molecule in order to foster the loss of nitric oxide (see the supplementary materials).[48] The rearrangement requires the rotation of the nitro group to form a CNO ring which is finally cleaved from the rest of the molecule.[11] A minimal energy geometry for this transition state was computed using the B3LYP/6-311++G* level of theory while calculations at the MP2 level failed to converge.

C. *Ab initio* calculations

Calculations at both the MP2 and TPSS-DFT level of theory suggest that the minimal energy geometry of neutral *p*NA has C_s symmetry where the benzene ring and the nitro group are essentially planar, but the amino group is pyramidal. However, the completely planar C_{2v} symmetrical conformation, which is a transition state with respect to the NH_2 wagging motion, is very close in energy (about 3 kJ/mol using TPSS and 1 kJ/mol using MP2). Comparing this to the frequency of the wagging motion, 540 cm^{-1} or 3.2 kJ/mol, it is apparent that this vibrational mode will be highly anharmonic, showing a large amplitude motion. Computing properties of the neutral accurately is thus challenging because it involves a weighted average over a large Franck-Condon zone and here we limit ourselves to reporting properties computed at the C_s and C_{2v} stationary points. It should be noted that these values will contribute strongly to the vibrationally averaged results. For the valence anion of *p*NA the situation is more straightforward: The electron occupies the lowest π^*-like orbital which increases the barrier associated with the amino wagging motion to 13.5 kJ/mol and while the valence anion may invert, it can clearly be thought of as having C_s symmetry. Note that due to the large spin contamination at the SCF level, MP2 calculations for the valence anion are expected to be unreliable, similar to what has been found for nitrobenzene.[49]

First, vertical electron attachment to *p*NA was studied with the EA-EOM-CCSD method using Aug-cc-pVDZ+ and Aug-cc-pVTZ+ basis sets. At both geometries the anion is predicted to have three bound states, two with EBE on the order of 100 meV, and one very weakly bound state with a binding energy of about 2 meV (Table II). The two states with approximately 100 meV binding energy represent a pair of strongly coupled diabatic states, one with dipole-bound and one with valence bound character; the third state is very diffuse and does not mix appreciably with the lower two states. The lower two states can be untangled at the planar geometry, because in C_{2v} symmetry the two states are decoupled with the dipole-bound state showing $^2A_1$ symmetry while the valence state has $^2B_1$ symmetry (Figure 6). The valence state is compact with an $\langle|r|\rangle$ value of 2.6 Å in contrast to the diffuse dipole bound state which has an $\langle|r|\rangle$ of 8.5 Å. As expected for a valence state, the EBE increases substantially in going from a double-zeta to a triple-zeta basis set (Table II). At non-planar geometries, the valence and dipole states mix

TABLE I. Dissociation barrier energies of $[p\text{NA-H}]^-$. Calculated energies are the difference between deprotonated *p*NA and the transition state.

Method	Loss of NO	Loss of NO_2^-
B3LYP/6-311++G*	0.99	4.30
MP2/Aug-cc-pVDZ	...	3.39
Experiment	2.36	3.80

TABLE II. Vertical electron affinities, in meV, computed with the EA-EOM-CCSD method. The standard augmented double-ζ and triple-ζ basis set were further augmented with a 6*s*6*p*6*d* set of extra diffuse functions at the center of mass of the molecule. At the C_{2v} symmetric transition state dipole-bound states have A_1 symmetry while the valence state has B_1 symmetry. In C_s symmetry all bound states have A′ symmetry, and only the third state can be characterized as dipole-bound, whereas the lower two states show a mixed character.

	C_{2v} symmetry		
	1st $^2A_1$	2nd $^2A_1$	1st $^2B_1$
Aug-cc-pVDZ+	104	2.0	47
Aug-cc-pVTZ+	107	2.0	208
	C_s symmetry		
	1st $^2A'$	2nd $^2A'$	3rd $^2A'$
Aug-cc-pVDZ+	110	80	1.5
Aug-cc-pVTZ+	261	96	1.5

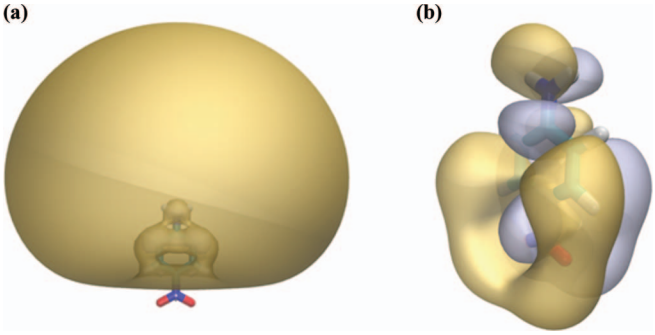

FIG. 6. Natural orbitals from EA-EOM-CCSD/Aug-cc-pVDZ+ calculations for the two lowest states of the *p*NA$^-$ anion. At the C_{2v} symmetrical transition state the two lower states of the anion have different symmetries, $^2A_1$ and $^2B_1$. Therefore, they are completely decoupled, and can be characterized as dipole-bound and valence. (a) shows the 80% enclosing iso-surface of the dipole-bound state and (b) shows the 90% enclosing iso-surface of the valence state. Note the different length scale of the two figures; $\langle|r|\rangle$ is 8.5 Å for the natural orbital of the dipole-bound state and just 2.6 Å for that of the valence state.

(both have $^2A'$ symmetry) with the state lower in energy being somewhat more compact and therefore having somewhat more valence character (Figure 7).

Second, the VDE of the *p*NA anion has been computed at its C_s symmetrical minimal energy structure and at the planar C_{2v} symmetrical transition state (Table III). The EA-EOM-CCSD/Aug-cc-pVTZ results suggest that the VDE depends strongly on the precise geometry of the NH_2 group, which in turn suggests that the VDE at the minimal energy structure may not be a reliable measure for the vibrationally averaged VDE (cf. discussion above). For a reliable prediction of the photoelectron spectrum, one would need to map out the VDE in the Franck-Condon zone and perform a Franck-Condon analysis for the anion to neutral transition. Moreover, finite temperature effects may be expected to shift the maximum of the photoelectron signal to lower energies because higher temperature should be associated with effectively planar NH_2 groups. Mapping and properly averaging the VDE

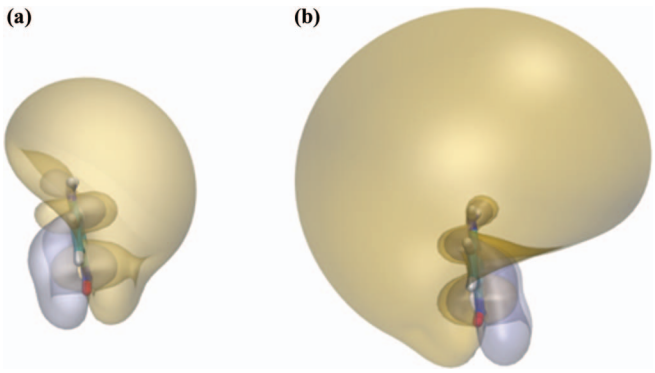

FIG. 7. Natural orbitals from EA-EOM-CCSD/Aug-cc-pVDZ+ calculations for the two lowest states of the *p*NA$^-$ anion. At the C_s symmetrical minimal energy geometry, the two lower states of the anion both have $^2A'$ symmetry are strongly coupled, and can not consequently be characterized as either dipole-bound or valence. Eighty-percent enclosing iso-surfaces of the first and second states are shown in (a) and (b), respectively. Note the comparable length scale of the two figures; $\langle|r|\rangle$ of the respective natural orbital is 4.3 Å for the lower and 6.8 Å for the higher state.

TABLE III. Vertical detachment energy, in eV, computed with different methods and basis sets. Two geometries are considered, the C_s symmetrical minimal energy structure of the *p*NA anion, and the associated C_{2v} symmetrical transition state of the NH_2 inversion.

		C_s minimum energy structure	C_{2v} transition state
Aug-cc-pVDZ	ΔCCSD(T)	0.83	0.69
	EA-EOM-CCSD	0.76	0.62
Aug-cc-pVTZ	ΔCCSD(T)	...	0.84
	EA-EOM-CCSD	0.94	0.80

are well beyond the scope of this paper, and again we have to limit ourselves to properties evaluated at stationary points, which suggest a VDE in the 0.85 to 1.0 eV range. This range is based on the ΔCCSD(T)/Aug-cc-pVTZ VDE of the C_{2v} symmetrical conformation, the energy difference between the C_{2v} and C_s symmetrical structure computed at the EOM-CCSD level, and the expectation that the Aug-cc-pVTZ basis set is reasonably well converged.

Finally, the adiabatic electron affinity (EA_a) for the valence *p*NA anion was calculated at the B3LYP/6-311++G* level using C_s geometry for the anion and C_{2v} for the neutral and the result is 0.88 eV. A presumably more reliable value for the EA_a of the valence state can be derived from (1) our best VDE (EOM-CCSD), (2) the CCSD(T) deformation energy of the neutral (that is, the energy difference of the neutral at its own equilibrium geometry and the neutral at the equilibrium geometry of the valence anion), and (3) the zero-point correction from the TPSS-DFT frequencies. Again, there are caveats regarding the floppy nature of the neutral, but for the EA_a these effects should be small. The EA_a obtained from the EOM-CCSD/Aug-cc-pVTZ VDE of 0.94 eV, the deformation energy of 0.32 eV (CCSD(T)/Aug-cc-pVTZ), and the zero-point correction of 0.11 eV (TPSS/maDef2-TVZP) is 0.73 eV. The biggest error likely arises from the VDE, which is, as discussed above, expected to be an underestimate. In any event, the value compares favorably with the experimental findings.

IV. CONCLUSIONS

Properties of the parent ion and the ion resulting from deprotonation of the highly polar p-nitroaniline molecule have been studied both experimentally and theoretically. The theoretical adiabatic electron affinity of *p*NA (0.73 eV) is in excellent agreement with the measured value of 0.75 ± 0.1 eV. Also, there is good agreement between theory and experiment for the dissociation energy leading to NO_2^- loss from [*p*NA − H]$^-$; however, combined theory and experiment predicts a significant barrier to the loss of NO from the dehydrogenated pNA anion.

In addition to the valence anions, we predicted two dipole-bound anion states, one at 100 meV and an excited state bound by about 2 meV. While there cannot be any doubt that *p*NA supports dipole-bound states, these states were not directly observed in this experiment. There are several reasons for this behavior: first, dipole-bound states are difficult to observe directly in such "doorway" cases as explained in our earlier studies of nitroethane,[50] nitromethane,[51] and

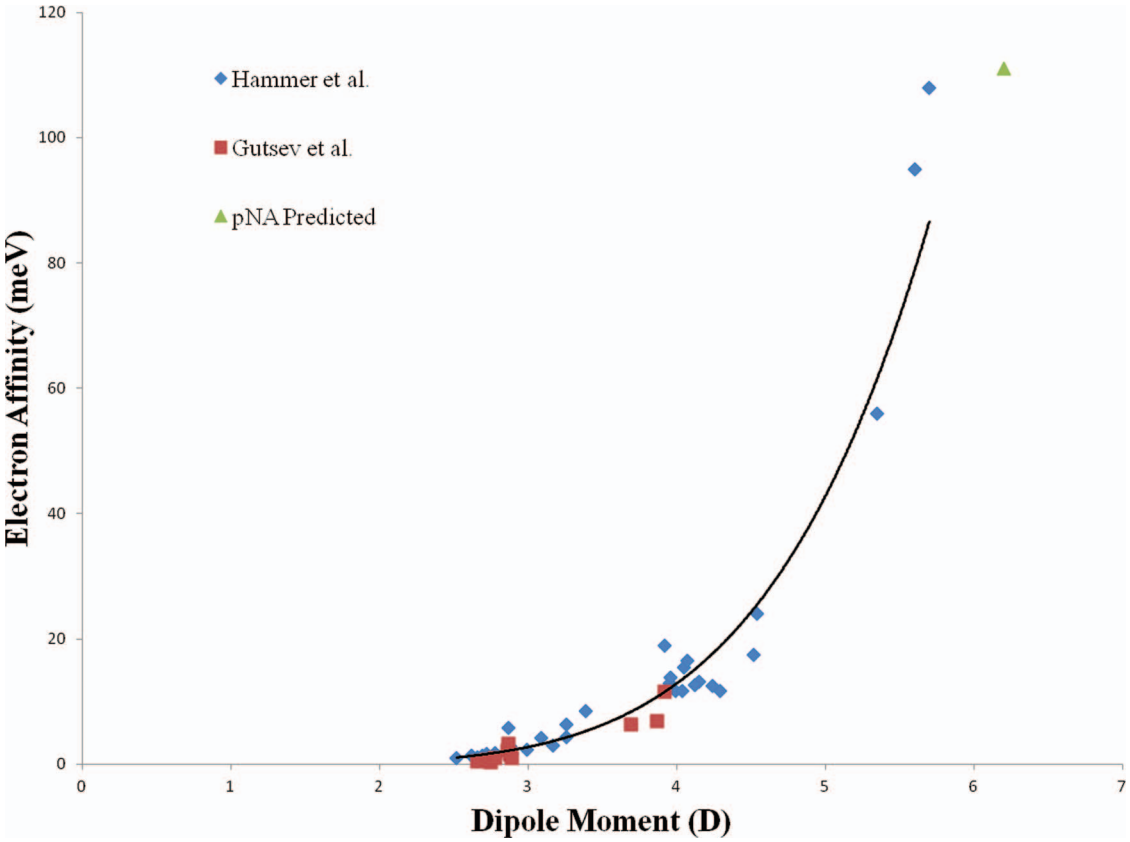

FIG. 8. A compilation of experimental electron binding energies versus molecular dipole moment.[52–57] There is some uncertainty as to the dipole moment of the isolated *p*NA molecule; however, it has been measured in acetone to be 6.2 D.[3]

nitrobenzene.[52] Second, we did not attempt to observe the dipole-bound anion of *p*NA with a predicted binding energy of 100 meV using Rydberg electron transfer (RET). Any formation of this dipole-bound anion using RET would occur at such low principle quantum numbers that signal would be too low to detect due to the inability of the ion-pair to separate as reported in earlier experiments with highly polar (∼5.5 D) molecules.[53] Also the dipole-bound state with an energy of 3 meV would be masked by the RET to the valence state much like that seen in our earlier studies.[50–52] Rotational resonances have been well studied previously for dipole-bound *radical anions*.[58,59] pNA^- represents an excellent candidate to search for threshold rotational resonances at both of the valence to dipole-bound excitation energies (i.e., $EA_a = 0.75$ eV or 1653 nm). The presence of two dipole bound states should make for interesting spectroscopy.

It is instructive to place the highly polar *p*NA molecule in reference to other dipole-bound anions. Figure 8 presents a comparison of all dipole-bound electron affinities reported from both experiment and theory versus dipole moment including our calculated value for *p*NA at 6.2 D. More experiments and theories are needed for polar molecules above 5 D in order to evaluate the molecular properties other than dipole moment which contribute to electron binding. For large dipole moment molecules, the electron is much "closer" to the molecular framework and at some point the electron can be bound into a valence type state. A solution to this problem for a high dipole moment molecule would be a better method used in the production of the dipole-bound anion. It is known that if the dipole moment is too high the detection of the anion is extremely difficult for Rydberg electron transfer processes due to the inability of the ion-pair to separate at such small internuclear separations.[51] To this end we are currently working on a method to accommodate fast Rydberg atoms in RET reactions to allow better separation of dipole-bound anion and alkali cation pairs to prepare dipole-bound anion signals intense enough for further studies.

Finally, we have previously pointed out that dipole-bound anions can act as "doorway states" to the formation of valence bound anions in nitroethane,[50] nitromethane,[51] and nitrobenzene.[52] One might call this intramolecular charge transfer within the molecule. This may be particularly important in large biomolecules (i.e., those involving amino acid moieties). In an extended system of such polar (or quadrupolar) molecules, electrons may flow from the dipole-bound state through the molecular framework to be stabilized on the electronegative end. Electrons might also be envisioned to pass through an extended chain of amino acids in a particular direction determined by the energy level of the dipole-bound anion (i.e. magnitude of the dipole moment). The works of Simons[60–62] and colleagues are beginning to address this important problem.

ACKNOWLEDGMENTS

Parts of this research are based on work supported by the National Science Foundation under Grant Nos. CHE-1111693 (K.H.B.) and CHE-0848487 (R.N.C.). We would also like to acknowledge the donors of The American Chemical Society Petroleum Research Fund for support of this research through Grant No. PRF 52486-UR6. We are indebted to Dr. Peter Armentrout for providing us with the CRUNCH program used in the supplementary materials.

[1]A. M. Moran, A. M. Kelley, and S. Tretiak, Chem. Phys. Lett. **367**, 293 (2003).
[2]H. S. Nalwa, M. Hanack, G. Pawlowski, and M. K. Engel, Chem. Phys. **245**, 17 (1999).
[3]L-T. Cheng, W. Tam, S. H. Stevenson, G. R. Meredith, G. Rikken, and S. R. Marder, J. Phys. Chem. **95**, 10631 (1991).
[4]H. Soscún, O. Castellano, Y. Bermúdez, C. Toro, N. Cubillán, A. Hinchliffe, and X. N. Phu, Int. J. Quantum Chem. **106**, 1130 (2006).
[5]A. Kawski, B. Kukliński, and P. Bojarski, Chem. Phys. **330**, 307 (2006).
[6]A. Hadjiantoniou, L. G. Christophorou, and J. G. Carter, J. Chem. Soc., Faraday Trans. 2 **69**, 1691 (1973).
[7]C. Huh, C. H. Kang, H. W. Lee, H. Nakamura, M. Mishima, Y. Tsuno, and H. Yamataka, Bull. Chem. Soc. Jpn. **72**, 1083 (1999).
[8]S. Chowdhury, H. Kishi, G. W. Dillow, and P. Kebarle, Can. J. Chem. **67**, 603 (1989).
[9]V. K. Potapov, I. E. Kardash, V. V. Sorokin, S. A. Sokolov, and T. I. Evlasheva, Khim. Vys. Energ. **6**, 392 (1972).
[10]P. Brown, Org. Mass Spectrom. **4**(suppl.), 533 (1970).
[11]J. H. Bowie, T. Blumenthal, and I. Walsh, Org. Mass Spectrom. **5**, 777 (1971).
[12]B. Gierczyk, J. Grajewski, and M. Zalas, Rapid Commun. Mass Spectrom. **20**, 361 (2006).
[13]D. M. Neumark, K. R. Lykke, T. Andersen, and W. C. Lineberger, Phys. Rev. A **32**, 1890 (1985).
[14]J. V. Coe, J. T. Snodgrass, C. B. Freidhoff, K. M. McHugh, and K. H. Bowen, J. Chem. Phys. **84**, 618 (1986).
[15]K. Do, T. P. Klein, C. A. Pommerening, and L. S. Sunderlin, J. Am. Soc. Mass Spectrom. **8**, 688 (1997).
[16]A. A. Hoops, J. R. Gascooke, A. E. Faulhaber, K. E. Kautzman, and D. M. Neumark, J. Chem. Phys. **120**, 7901 (2004).
[17]R. M. Lynden-Bell, R. Kosloff, S. Ruhman, D. Danovich, and J. Vala, J. Chem. Phys. **109**, 9928 (1998).
[18]F. A. Khan, D. E. Clemmer, R. H. Schultz, and P. B. Armentrout, J. Phys. Chem. **97**, 7978 (1993).
[19]F. Muntean and P. B. Armentrout, J. Chem. Phys. **115**, 1213 (2001).
[20]J. C. Amicangelo and P. B. Armentrout, Int. J. Mass Spectrom. **212**, 301 (2001).
[21]P. B. Armentrout, K. M. Ervin, and M. T. Rodgers, J. Phys. Chem. A **112**, 10071 (2008).
[22]N. F. Dalleska, K. Honma, L. S. Sunderlin, and P. B. Armentrout, J. Am. Chem. Soc. **116**, 3519 (1994).
[23]M. T. Rodgers, K. M. Ervin, and P. B. Armentrout, J. Chem. Phys. **106**, 4499 (1997).
[24]T. Beyer and D. F. Swinehart, Commun. ACM **16**, 379 (1973).
[25]S. J. Nalley, R. N. Compton, H. C. Schweinler, and V. E. Anderson, J. Chem. Phys. **59**, 4125 (1973).
[26]S. Narancic, A. Bach, and P. Chen, J. Phys. Chem. A **111**, 7006 (2007).
[27]J. Tao, J. P. Perdew, V. N. Staroverov, and G. E. Scuseria, Phys. Rev. Lett. **91**, 146401 (2003).
[28]F. Weigend and R. Ahlrichs, Phys. Chem. Chem. Phys. **7**, 3297 (2005).
[29]E. Papajak and D. G. Truhlar, J. Chem. Theory. Comput. **6**, 597 (2010).
[30]T. H. Dunning, Jr., J. Chem. Phys. **90**, 1007 (1989).
[31]R. A. Kendall, T. H. Dunning, Jr., and R. J. Harrison, J. Chem. Phys, **96**, 6796 (1992).
[32]M. J. Frisch, G. W. Trucks, H. B. Schlegel *et al.*, GAUSSIAN 09, Revision B.01, Guassian, Inc., Wallingford, CT, 2009; GAUSSIAN 03, Revision 6.0, Gaussian, Inc., Wallingford, CT, 2003.
[33]F. Neese, with contributions from U. Becker, D. Ganiouchine, S. Koßmann, T. Petrenko, C. Riplinger and F. Wennmohs, ORCA, version 2.8.0, 2010; an updated version is available at http://www.mpibac.mpg.de/bac/logins/neese/description.php.
[34]J. F. Stanton, J. Gauss, M. E. Harding, P. G. Szalay, with contributions from A. A. Auer, R. J. Bartlett, U. Benedikt, C. Berger, D. E. Bernholdt, Y. J. Bomble, L. Cheng, O. Christiansen, M. Heckert, O. Heun, C. Huber, T.-C. Jagau, D. Jonsson, J. Jusélius, K. Klein, W. J. Lauderdale, D. A. Matthews, T. Metzroth, L. A. Mück, D. P. O'Neill, D. R. Price, E. Prochnow, C. Puzzarini, K. Ruud, F. Schiffmann, W. Schwalbach, S. Stopkowicz, A. Tajti, J. Vázquez, F. Wang, J. D. Watts and the integral packages *MOLECULE* (J. Almlöf and P. R. Taylor), *PROPS* (P. R. Taylor), *ABACUS* (T. Helgaker, H. J. Aa. Jensen, P. Jørgensen, and J. Olsen), and ECP routines by A. V. Mitin and C. van Wüllen, CFOUR version 1, 2010. For the current version, see http://www.cfour.de.
[35]N. I. Hammer, K. Diri, K. D. Jordan, C. Defrançois, and R. N. Compton, J. Chem. Phys. **119**, 3650 (2003).
[36]K. M. Ervin and P. B. Armentrout, J. Chem. Phys. **83**, 166 (1985).
[37]M. E. Weber, J. L. Elkind, and P. B. Armentrout, J. Chem. Phys. **84**, 1521 (1986).
[38]R. H. Schultz, K. C. Crellin, and P. B. Armentrout, J. Am. Chem. Soc. **113**, 8590 (1991).
[39]A. A. Shvartsburg, K. M. Ervin, and J. H. Frederick, J. Chem. Phys. **104**, 8458 (1996).
[40]V. F. DeTuri and K. M. Ervin, J. Phys. Chem. A **103**, 6911 (1999).
[41]C. Iceman and P. B. Armentrout, Int. J. Mass Spectrom. **222**, 329 (2003).
[42]T. Su, J. Chem. Phys. **100**, 4703 (1994).
[43]K. M. Ervin, Int. J. Mass Spectrom. **185**, 343 (1999).
[44]H. Koizumi and P. B. Armentrout, J. Chem. Phys. **119**, 12819 (2003).
[45]H. Koizumi, F. Muntean, and P. B. Armentrout, J. Chem. Phys. **120**, 756 (2004).
[46]J. C. Amicangelo and P. B. Armentrout, J. Phys. Chem. A **108**, 10698 (2004).
[47]P. B. Armentrout, J. Chem. Phys. **126**, 234302 (2007).
[48]See supplementary materials at http://dx.doi.org/10.1063/1.4810869 for detailed information about the CID modeling.
[49]J. Lambert, J. Chen, A. Buonaugurio, K. H. Bowen, C.-L. Do-Thanh, Y. Wang, M. D. Best, R. N. Compton, and T. Sommerfeld, "Combined photoelectron, collision-induced dissociation, and computational studies of parent and fragment anions of N-paranitrosulfophenylsufonyalanine and N-paranitrophenylalanine," J. Chem. Phys. (unpublished).
[50]S. T. Stokes, K. H. Bowen, T. Sommerfeld, S. Ard, N. Mirsaleh-Kohan, J. D. Steill, and R. N. Compton, J. Chem. Phys. **129**, 064308 (2008).
[51]R. N. Compton, H. S. Carman, Jr., C. Defrancois, J. H. Hendricks, S. A. Lyapustina, and K. H. Bowen, J. Chem. Phys. **105**, 3472 (1996).
[52]C. Desfrancois, V. Périquet, S. A. Lyapustina, T. P. Lippa, D. W. Robinson, K. H. Bowen, H. Nonaka, and R. N. Compton, J. Chem. Phys. **111**, 4569 (1999).
[53]N. I. Hammer, R. J. Hinde, R. N. Compton, K. Diri, K. D. Jordan, D. Radisic, S. T. Stokes, and K. H. Bowen, J. Chem. Phys, **120**, 685 (2004).
[54]G. L. Gutsev and L. Adamowicz, Chem. Phys. Lett. **235**, 377 (1995).
[55]R. D. Nelson, Jr., D. R. Lide, Jr., and A. A. Maryott, *Selected Values of Electric Dipole Moments for Molecules in the Gas Phase*, NSRDS-NBS, Vol. 10 (US GPO, Washington, 1967).
[56]D. R. Lide, ed., *CRC Handbook of Chemistry and Physics* (CRC Press, Boca Raton, 1994).
[57]C. Desfrançois, H. Abdoul-Carime, N. Khelifa, and J. P. Schermann, Phys. Rev. Lett. **73**, 2436 (1994).
[58]A. S. Mullins, K. K. Murray, C. P. Schultz, and W. C. Lineberger, J. Phys. Chem. **97**, 10281 (1995).
[59]E. A. Brinkman, S. Berger, J. Marks, and J. I. Brauman, J. Chem. Phys. **99**, 7586 (1993).
[60]M. Gutowski, P. Skurski, and J. Simons, Int. J. Mass Spectrom. **201**, 245 (2000).
[61]J. Simons, J. Am. Chem. Soc. **132**, 7074–7085 (2010).
[62]D. Neff and J. Simons, J. Phys. Chem. A **114**, 1309–1323 (2010).